Nanoscale

PAPER

View Article Online
View Journal | View Issue

Cite this: *Nanoscale*, 2016, **8**, 12639

Monodispersed calcium carbonate nanoparticles modulate local pH and inhibit tumor growth *in vivo*†

Avik Som,[a,b] Ramesh Raliya,[c] Limei Tian,[d] Walter Akers,[a] Joseph E. Ippolito,[a] Srikanth Singamaneni,[d] Pratim Biswas[c] and Samuel Achilefu*[a,b]

Received 8th September 2015,
Accepted 24th December 2015

DOI: 10.1039/c5nr06162h

www.rsc.org/nanoscale

The acidic extracellular environment of tumors potentiates their aggressiveness and metastasis, but few methods exist to selectively modulate the extracellular pH (pHe) environment of tumors. Transient flushing of biological systems with alkaline fluids or proton pump inhibitors is impractical and nonselective. Here we report a nanoparticles-based strategy to intentionally modulate the pHe in tumors. Biochemical simulations indicate that the dissolution of calcium carbonate nanoparticles (nano-$CaCO_3$) *in vivo* increases pH asymptotically to 7.4. We developed two independent facile methods to synthesize monodisperse non-doped vaterite nano-$CaCO_3$ with distinct size range between 20 and 300 nm. Using murine models of cancer, we demonstrate that the selective accumulation of nano-$CaCO_3$ in tumors increases tumor pH over time. The associated induction of tumor growth stasis is putatively interpreted as a pHe increase. This study establishes an approach to prepare nano-$CaCO_3$ over a wide particle size range, a formulation that stabilizes the nanomaterials in aqueous solutions, and a pH-sensitive nano-platform capable of modulating the acidic environment of cancer for potential therapeutic benefits.

Introduction

The current understanding of cancer development has evolved from a simple view of uncontrolled growth stemming from gene mutation within a single cell to that of complex interactions between different cell types and their local chemical environment. In particular, the 4–5 fold increase in the extracellular hydrogen ion concentration around tumor cells, previously considered a byproduct of upregulated glycolysis, appears to support elevated tumor growth, immune evasion, and metastasis.[1–5] To combat these effects, various cancer therapies focusing on modulating extracellular pH (pHe) of tumors have been investigated.[6] For instance, intracellular modulators of intrinsic proton transport and production such as proton pump and carbonic anhydrase IX inhibitors have inhibited tumor growth by increasing pH *in vivo*.[1,6,7] However, the intracellular targets of these drugs are expressed in non-cancerous cells and therefore can have off-target toxic effects.[7] In addition, redundancy of intracellular pathways can lead to drug resistance and loss of therapeutic efficacy over time.[8,9]

To avoid intracellular resistance pathways, dietary alterations including sodium bicarbonate can raise the systemic extracellular pH.[2] Although a positive response has been observed in some tumors, this approach requires the administration of large amounts of the salt, does not target the tumors directly, has a transient effect on tumor pHe because of the rapid clearance from circulation, and is expected to induce metabolic alkalosis and consequent morbidity.[10]

An alternative approach to directly modulate the acidic pHe of tumors is to develop nanoparticle delivery vehicles with sustainable buffering capacity. This approach could minimize the drug resistance potential seen in intracellular therapies, but also add the selectivity seen with nanotechnology.[11] Cationic secondary amine dendrimers have been used to respond to acidic pH, mainly to escape the lysosome, for intracellular drug delivery.[12] However, dendrimers are capable of neutralizing only a small number of protons (10^{-20} mole) per nanoparticle, thereby limiting their buffering capacity. Unless a

[a]*Departments of Radiology, Washington University School of Medicine, St. Louis, Missouri, USA. E-mail: achilefus@mir.wustl.edu*
[b]*Department of Biomedical Engineering, Washington University, St. Louis, Missouri, USA*
[c]*Department of Energy, Environmental and Chemical Engineering, Washington University, St. Louis, Missouri, USA*
[d]*Department of Mechanical and Materials Science Engineering, Washington University, St. Louis, Missouri, USA*

†Electronic supplementary information (ESI) available: Summary of experiments, theoretical schema of effect, synthesis schema, X-Ray diffraction results, TEM of effects of different solvents on particles in various solvents. See DOI: 10.1039/c5nr06162h

non-desirable continuous infusion of the polyamine nanoparticles is used, their buffering capacity is not regenerative, and the products of amine protonation could induce off-target toxicity. Inorganic nanoparticles, such as doped $CaCO_3$, have been used for acid sensitive drug release.[13,14] However, rarely has any biocompatible inorganic nanoparticle been intentionally designed and used to modulate tumor pHe.

In this work, we developed methods to prepare monodisperse nano-$CaCO_3$ with size ranges from 20–300 nm. We also identified a method to stabilize the materials in aqueous media. Simulations and *in vitro* testing show that regenerative buffering capacity is obtained because the products of this interaction, water and bicarbonate, dissociate from the bulk nanoparticle core, creating a new surface to neutralize additional protons produced by the cells. In addition, we demonstrate that nano-$CaCO_3$ with distinct sizes can selectively localize in the extracellular region of tumors and modulate tumor pH in rodents, accompanied by the prevention or reduction of tumor growth (Fig. S1†).

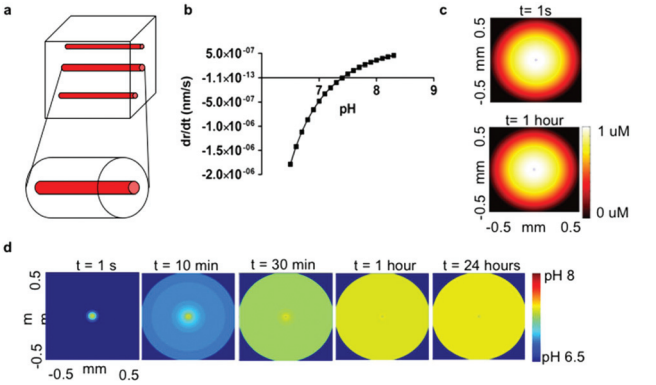

Fig. 1 Simulation of $CaCO_3$ dissolution *in vivo* predicts tumor pHe will increase only to 7.4. (a) Tissue can be simulated as a series of cylindrical capillaries each supplying a larger cylindrical volume of tissue. (b) Rate of change in size of $CaCO_3$ particle reaches an equilibrium at pH = 7.4 under *in vivo* conditions. (c) The distribution of 100 nm $CaCO_3$ nanoparticles in a circular cross section is simulated to reach ~0.5 mm away from the capillary with constant infusion and degrades minimally over 60 minutes. (d) Spatial pH distribution over time increases from 6.5 to 7.4 by 60 minutes, and remains at 7.4 for at least 24 h. Capillary source is represented by blue circle in both (c) and (d).

Results and discussion

Simulation of $CaCO_3$ nanoparticle dissolution *in vivo* predicts asymptotic pH increase and buffering to pH 7.4

$CaCO_3$ is an important biomaterial that is widely available in different forms. Although $CaCO_3$ solutions can serve as buffering agents, a saturated aqueous solution of this salt has a predicted pK_a of about 9, suggesting the potential to induce metabolic alkalosis *in vivo*. In the solid state, $CaCO_3$ exists predominantly as calcite, aragonite, or vaterite polymorphs. Each of these polymorphs differs in their crystal lattice structure. Unlike calcite and aragonite, which are not soluble in aqueous medium, vaterite is more soluble because of its low thermodynamic stability compared to the other polymorphs found in nature. For our intended application, slow but consistent dissolution in mildly acidic solutions is an essential criterion for a regenerative pHe buffering agent. To prevent metabolic alkalosis in surrounding healthy tissue, the preferred material should only increase the pH to about 7.4 (normal body pH).

Because $CaCO_3$ dissolution is regulated by basic rate equations, a simulation of its dissolution and prediction of the expected pH changes *in vivo* and *in vitro* is possible (Fig. 1). Dissolution of $CaCO_3$ under mildly acidic conditions follows several steps:

$$CaCO_3(s) \leftrightharpoons Ca^{2+} + CO_3{}^{2-} (k_{a1} = 4.45 \times 10^{-7}) \quad (1a)$$

$$H_2O + HCO_3{}^- \leftrightharpoons H_3O^+ + CO_3{}^{2-} (k_{a2} = 4.69 \times 10^{-11}) \quad (1b)$$

$$H_2O + H_2CO_3 \leftrightharpoons H_3O^+ + HCO_3{}^- \quad (1c)$$

Generation of carbonate in eqn (1) drives $CaCO_3$ dissolution under acidic pH conditions following L'Chatelier's principle. Previous studies have modeled the pH changes in response to $CaCO_3$ dissolution in an aqueous medium.[15] Adapting this model to a tissue cylinder approach (Fig. 1a), we derived the following equations:

$$C_b = \sqrt{\frac{K_{sp}}{K_{a1} \times K_{a2}}} \Big/ \sqrt{\left((10^{-pH})^2 + K_{a1}10^{-pH} + K_{a1}K_{a2}\right)} \quad (2)$$

$$J = -D\frac{dC}{dx} \rightarrow \frac{\partial C}{\partial t} = \frac{A}{V}D\frac{(C_s - C_b)}{d} \rightarrow \frac{\partial m}{\partial t} = AD\frac{(C_s - C_b)}{d} \rightarrow \frac{\partial r_p}{\partial t} = \frac{D}{\rho}\frac{(C_s - C_b)}{d} \quad (3)$$

$$\frac{dpH}{dt} = -\frac{D}{B}\frac{(C_s - C_b)}{d} \times \frac{1}{L} \quad (4)$$

The solubility of $CaCO_3$ (C_b) is a function of the solubility product (K_{sp}), pH, and the equilibrium constants (K_{a1} and K_{a2}). Change in concentration of $CaCO_3$ is a function of the $CaCO_3$ concentration (C_s), the solubility (C_b), the surface area (A), the diffusion distance (d), and volume (V). The radius of the particle (r_p) is additionally dependent on the density of $CaCO_3$ (ρ). The change in pH is also dependent on the buffering constant, and approximates A/V as $1/L$, where L is the length of the tissue cylinder. Using eqn (2)–(4), an equilibration point occurs for dissolving $CaCO_3$ at a pH of 7.4 (Fig. 1b). This suggests that $CaCO_3$ will only increase pH in acidic environments such as those found in the pHe of solid tumors and that this process is unlikely to induce metabolic alkalosis because the pH will not exceed 7.4.

To visualize this process in a 3D model, we modeled nano-$CaCO_3$ diffusion in a tissue matrix using a tissue cylinder model (Fig. 1a), where a single capillary is assumed to feed a tissue cylinder. From this model, we derived the equation for

the distribution of $CaCO_3$ in the tissue cylinder as a function of the radius (r), capillary radius (r_c), diffusion coefficient of $CaCO_3$ (D_c), the partition coefficient (k), degradation rate (R_{cmax}), and the influx dose (C_d) as follows:

$$[CaCO_3] = \frac{R_{cmax}}{4D_c}\left(r_c^2 - r^2\right) + \frac{R_{cmax}r_c^2}{2D_c}\ln\left|\frac{r}{r_c}\right| + k \cdot C_d \quad (5)$$

The diffusion coefficient (D_c) of the particle in tissue, which is dependent on particle size, was estimated using the Renkin equation.[16] We also derived the initial pH distribution from diffusion of protons from the capillary to be the following as a function of the rate of proton production (R_{pmax}), diffusion of the proton (D_p), radius (r), and capillary radius (r_c):

$$[H^+] = \frac{R_{pmax}}{4D_p}\left(r^2 - r_c^2\right) + \frac{R_{pmax}r_c^2}{2D_p}\ln\left|\frac{r_c}{r}\right| + 10^{-7.4} \quad (6)$$

The change in proton concentration is thus determined by numerically solving eqn (2), (4), and (6) by iteration. Similarly, $CaCO_3$ concentrations can be calculated by using a combination of eqn (2), (3), and (5) over the associated tissue cylinder. We find that the $CaCO_3$ concentrations are relatively constant over time, predicting a slow dissolution process (Fig. 1c). In addition, the simulation predicts that the pH does not exceed its maximum of 7.4 by 24 h (Fig. 1d). This profile predicts that *in vivo* $CaCO_3$ dissolution is acid selective and therefore is an ideal nanomaterial for modulating the acidic pHe of solid tumors. Additional information on the derivation of the equations and model assumptions can be found in the ESI.†

Independent facile synthetic methods produce pure vaterite nanoparticles with controlled size range from 20–300 nm

The malformation of blood and drainage vessels around solid tumors creates an environment for the selective retention of nanoparticles through the enhanced permeation and retention (EPR) effect.[17] Typically, materials with core diameters less than 500 nm are preferred to enhance intravascular dynamics and diffusion to tumor cells further from the blood vessels.[11,17]

Unfortunately, $CaCO_3$ nanoparticles that are stable in aqueous solutions have been difficult to synthesize at sub-micron sizes without the use of harsh conditions (custom high pressure systems), doping materials (lipid-based surfactants), other additives such as phosphate, polystyrene, and drugs, or a combination of calcium phosphate and calcium carbonate.[13,14,18–20] Attempts to prepare pure nano-$CaCO_3$ have generally resulted in the production of materials with core diameter >500 nm (ref. 21–23) due to difficulty in controlling the particle's growth. Furthermore, $CaCO_3$ nanoparticles can rapidly grow to larger crystalline polymorphs (calcite, vaterite, or aragonite) when placed under aqueous conditions *via* a variety of mechanisms.[24–28]

Building on literature methods, we have identified two independent methods to produce pristine sub-micron vaterite nano-$CaCO_3$ with distinct size ranges at 20 nm, 100 nm, and 300 nm. Synthesis of the 100 nm nano-$CaCO_3$ was accomplished by using a gas diffusion method (Fig. S2,† Methods section).[24] The stepwise approach of exposing calcium chloride in anhydrous ethanol to controlled amounts of ammonium bicarbonate, followed by gradual air drying of the product, afforded a simple and highly reproducible method to prepare these nanoparticles. To provide flexibility in particle size, we used a double decomposition reaction method between hydrated calcium chloride and sodium bicarbonate at room temperature. Size control was achieved by mixing the reactants in a mixture of solvents consisting of 1 : 5 ratio of water/polyethylene glycol (20 nm) and water/ethylene glycol (300 nm). The ethylene glycol and polyethylene glycol were used to modulate the diffusion rate of calcium and carbonate ions, thereby controlling nucleation and growth by particle cluster formation.[29,30] This approach revealed that solvent viscosity can serve as a modular strategy to prepare pure vaterite nanoparticles.

The size and morphology of synthesized nano-$CaCO_3$ were determined by transmission electron microscopy (TEM) and dynamic light scattering (DLS) (Fig. 2). Typical TEM micrographs revealed that nano-$CaCO_3$ were primarily spherical, as expected for vaterite. The geometric mean diameters of the nano-$CaCO_3$ were 20 ± 1.4 nm, 100 ± 8.3 nm and 300 ± 14.6 nm (Fig. 2a–c). Expectedly, DLS revealed a slight increase in the hydrodynamic diameter (D_h) for all particle sizes because of the interaction of solvent molecules with the surface of particles, creating a thin layer of solvent molecules (Fig. 2d).

However, two peaks were observed in the DLS profile of the 20 nm nanoparticles, in which one peak exhibited smaller D_h

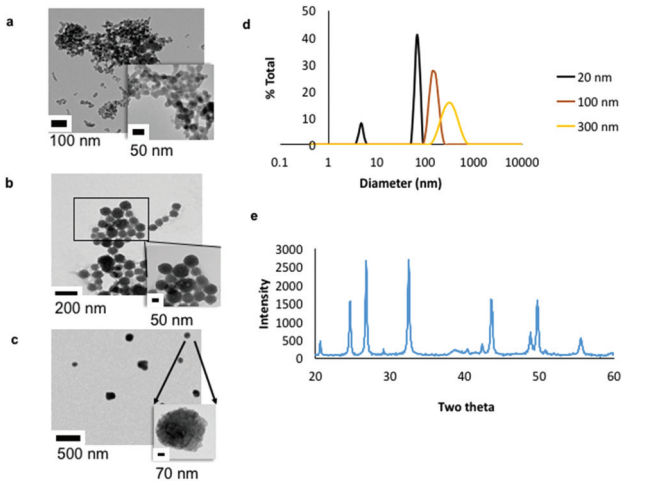

Fig. 2 Independent facile synthesis methods can produce nano-$CaCO_3$ at various sizes. (a) TEM of 20 nm vaterite demonstrates rod-like particles with a tendency for aggregation. (b) TEM of 100 nm vaterite shows spherical particles. (c) TEM for 300 nm vaterite demonstrates larger spherical particles. (d) DLS results in ethanol for the 3 particle sizes replicates TEM findings. (e) XRD of 100 nm $CaCO_3$ demonstrates vaterite signature.

than the physical diameter. These peaks could arise from the asymmetric shape of the particles, as shown in the 20 nm particles (Fig. 2a).[31] Larger sizes were typically spherical, accounting for the lack of a second smaller peak. Irrespective of the synthesis method, all three sizes of the nano-$CaCO_3$ showed peaks at theta angles of 24.8, 27.1, 32.8 and 43.9, which are consistent with the characteristic hexagonal vaterite crystalline structure of $CaCO_3$ (Fig. 2e and S3†). Because vaterite is more soluble in aqueous media than other $CaCO_3$ polymorphs, these materials are suitable for use in alkalinizing the acidic pHe of tumors if they can remain stable in aqueous environments without rapidly converting to the less soluble calcite.

Albumin prevents rapid conversion of vaterite nanoparticles to calcite or calcium phosphate in aqueous medium and serum

The solubility and stability of these vaterite nanoparticles are critical for successful biological applications *in vivo*. We explored a variety of biologically compatible media to identify the optimal storage conditions and vector for intravenous (I.V.) administration of the nano-$CaCO_3$ (Fig. 3; Fig. S4†). DLS analysis shows a rapid increase of the 100 nm vaterite nanoparticles from 100 nm to over 500 nm within a few seconds in saline and phosphate buffered saline (PBS; Fig. 3a). The observed morphological change in PBS could be attributed to calcite or $CaPO_4$ formation. However, the addition of 2% albumin in PBS remarkably stabilized the materials for extended periods, demonstrating the potential of formulating vaterite nanoparticles in this medium for I.V. administration (Fig. 3a and b). A similar trend was observed with the 20 nm and 300 nm nano-$CaCO_3$ (Fig. S5†).

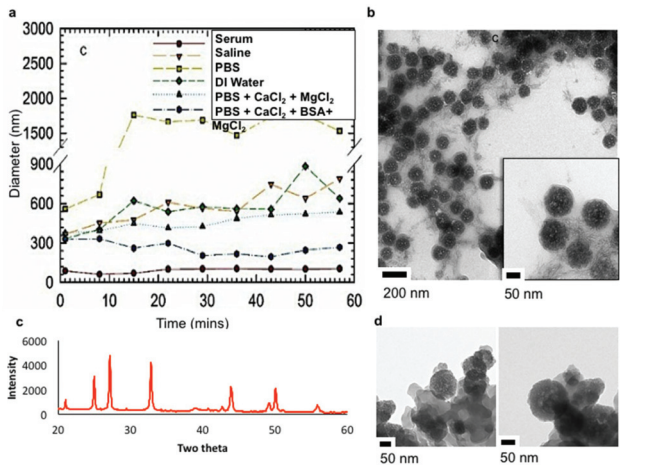

Fig. 3 Nano-$CaCO_3$ is stabilized in an albumin-based solution. (a) DLS results of 100 nm particles show that stability in serum > PBS + BSA + $CaCl_2$ > PBS + $CaCl_2$ > Saline = DI Water > PBS. (b) TEM shows 100 nm particles in albumin solution have unchanged morphology surrounded by albumin. (c) XRD of 100 nm particles in albumin solution at 24 h shows no changes in crystalline structure. (d) TEM of particles post serum incubation demonstrates no change in structure, with particles embedded in serum protein.

We further determined the long-term particle stability in different media for up to 7 h. Time-resolved DLS (TR-DLS) suggests that the particles in aqueous albumin-containing solution exist in pairs of 2 or 3 (size 2–3 times larger than in ethanol), which dissociate into individual particles upon exposure to fetal serum (Fig. 3a, S5†). TEM confirmed the high stability of the particles in albumin solution (Fig. 3b, S5†). X-Ray Diffraction (XRD) analysis did not show any change in crystallinity in albumin-based aqueous media (Fig. 3c). The nano-$CaCO_3$ exhibited stability in both morphology and size in fetal bovine serum (Fig. 3d, 5).

These results suggest that albumin, which has a high affinity for calcium,[32] serves as a calcium sink that prevents aggregation and calcium phosphate formation in PBS. The minimal change in TEM (structural) and X-ray diffraction (crystalline) analyses confirms that extensive double replacement to form $CaPO_4$ did not occur. In general, clusters of three nano-$CaCO_3$ form in albumin solutions, which separate into single particle serum is added to the mixture. The additional serum stability conferred on nano-$CaCO_3$ in aqueous albumin solution indicates that pre-formulation of the nanoparticles in this medium is ideal for *in vivo* application, where serum is abundant.

Efficacy of modulating the acidic pH of tumors *in vivo* depends on $CaCO_3$ nanoparticle size

Predicated on the simulation studies, we assessed the buffering capacity of the nanoparticles in cell-free media under 5% CO_2 and hypoxic (0.3% O_2) conditions (Fig. 4a). In non-acidified conditioned media (pH 7.4), the solution pH was largely unchanged in the presence of different sizes and concentrations of vaterite nano-$CaCO_3$, as predicted by simulations above. However, treatment of acidic conditioned media (pH 6.2) with any of the particles (0.67 mg mL^{-1}) showed a

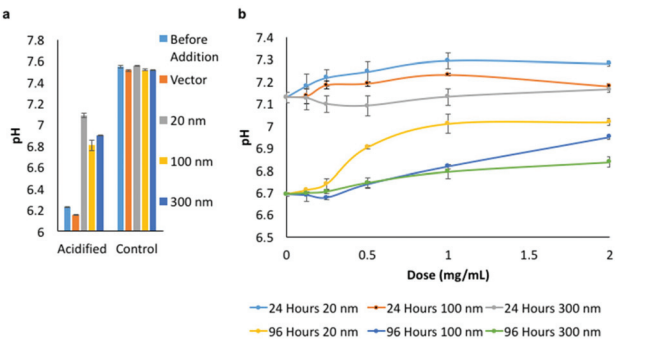

Fig. 4 Nano-$CaCO_3$ increases pH up to 7.4 *in vitro*. (a) pH change in media at 5% CO_2 shows a significant increase in pH when using particles as compared to vector alone. All solutions were added in 10 μL solvent (2% albumin + PBS with $CaCl_2$ and $MgCl_2$). (b) pH change *versus* dose when incubated with HT1080 (human fibrosarcoma) cells using different particle sizes shows an increase in pH with one dose of $CaCO_3$, as well as a differential effect on pH at later time points of growth depending on size. Error bars refer to the standard error across n = 3 biologic replicates.

rapid increase in pH, which did not exceed 7.2. Similarly, the pH remained at about pH 7.2 after 24 h incubation of human fibrosarcoma (HT1080) cells in normal cell culture conditions, irrespective of the nanoparticle doses used (Fig. 4b). At 96 h post HT1080 cellular induced acidification, nanoparticle size-dependent pH changes were observed, with the 20 nm materials having the highest increase in pH. This trend could be attributable to the higher diffusion rate and the larger surface area of the 20 nm nano-$CaCO_3$.

Despite recent advances in noninvasive methods to measure pH, they still suffer from poor sensitivity to pHe and poor temporal resolution needed to measure the dynamic changes in pH.[33] Our initial attempt to determine tumor pHe by the reported ^{31}P NMR spectroscopic technique using 3-aminopropylphosphonate[34] was unsuccessful due to technical issues. To determine whether nano-$CaCO_3$ was capable of altering pH *in vivo*, we used a 5 mm diameter invasive *in vivo* pH electrode probe (Fig. 5a), and putatively interpreted the resulting pH values as predominantly extracellular. Based on this technique Based on this technique, we find that a control vector administration resulted in a slight decrease in pH over time, possibly due to a variety of factors that may include cell lysis, blood vessel destruction, and inflammation from the probe injury. Against this background, I.V. administration of 1 mg bolus injections of each of the 3 types of nano-$CaCO_3$ in HT1080 tumor-bearing mice increased the tumor pH for over 3 h at varying amounts. The 100 nm nano-$CaCO_3$ showed the highest ΔpH and longest effect (Fig. 5b). The 20 nm particles appeared to diffuse into and out of the tumor area more rapidly than the 100 nm particles.

Intuitively, larger particles are expected to exert higher response because of their favorable EPR effect. However, the 300 nm nano-$CaCO_3$ do not appear to appreciably increase the pH of tumors. The poor diffusion of these particles dictates that they can only exert an effect in a small section of a three-dimensional tumor environment. Our data also show that flooding the mouse with a high concentration (0.3–0.4 g kg^{-1}) of sodium bicarbonate (~10× the nanoparticle I.V. dosage) did not induce a measurable pH change in the tumor region (Fig. 5b), which may be due to rapid clearing by the kidney and lungs.

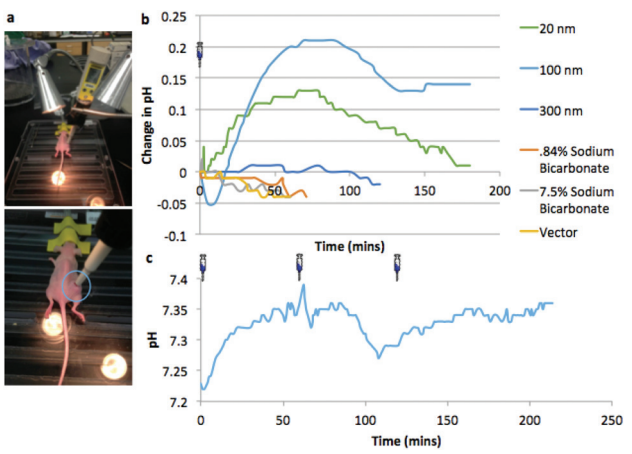

Fig. 5 I.V. injections of nano-$CaCO_3$ increase tumor pH *in vivo* up to 7.4. (a) Image of pH measurement setup. The probe is ~5 mm deep into the tumor, and ~5 mm wide, suggesting that any pH value measured is most likely extracellular. (b) pH change *in vivo* with 1 mg bolus intravenous injections (time point of injection symbolized on the graph as an injection needle) of $CaCO_3$ particles, bicarbonate, or vector. (c) pH change with multiple injections of 100 nm particles in HT1080 tumor models demonstrates asymptotic changes near pH of 7.4.

Transient alkalinization of the acidic pHe can inhibit tumor growth

The effect of persistent alkalinization of the acidic pHe of solid tumors is not known at this time. Dynamic pH measurements in mice bearing HT1080 tumors indicate that 100 nm sized nanoparticles administered at a bolus dose of 1 mg (0.04–0.05 g per kg body weight) almost linearly increases the pH during the first 30 minutes, followed by a decrease at about 100 minutes. Repeated dosing at selected time points can maintain the pH close to 7.4 (Fig. 5c), which matches the expectations of our simulation (Fig. 1).

Consistent with our hypothesis, we found that repeated daily administration of nano-$CaCO_3$ significantly inhibited tumor growth (Fig. 6a and b). Further, discontinuation of the nano-$CaCO_3$ treatment partially reversed this trend, resulting in the acceleration of tumor growth rate (Fig. 6c and d). This finding suggest the potential of tumor cell reprograming in response to an initial assault by nano-$CaCO_3$. Future studies will explore this concept. Our results suggest that if a thera-

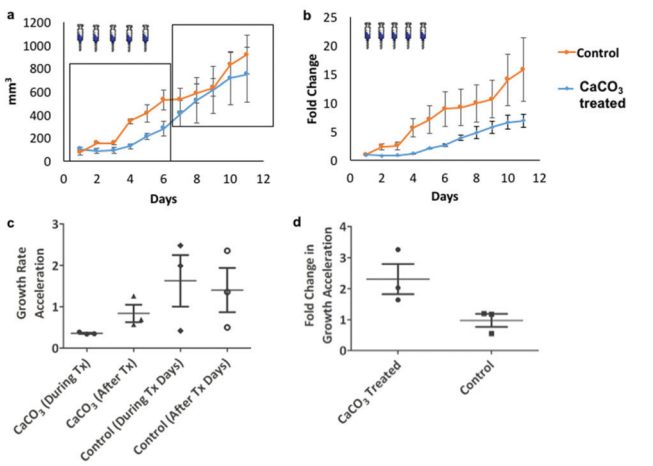

Fig. 6 Repeated administration of 100 nm nano-$CaCO_3$ inhibits tumor growth *in vivo*. (a) Tumor size during treatment (first box) is significantly lower than control, which partially equalizes after treatment ends (second box). (b) Controlling for initial size, the fold change in tumor size is significantly reduced in treated tumors. (c) Growth rate of treated tumors is decreased compared to control during treatments and only partially returns to normal after treatment removal. (d) Removal of $CaCO_3$ doubled the growth rate acceleration of the tumor after treatment removal, with little change in control over the same period. Error bars represent standard error. Error bars refer to standard error with n = 3 biologic replicates for each arm.

peutic outcome using this method is envisaged, multiple doses of nano-$CaCO_3$ may be required to sustain the alkalinizing effect until either depletion of the nanoparticles or reprogramming of the tumor cells in response to treatment. To achieve a sustainable tumor-inhibitory effect, it will be necessary to optimize dosing, combine nano-$CaCO_3$ with other therapies, and improve targeting of the nano-$CaCO_3$ to tumors.

Conclusions

We have identified a facile, scalable method for mass production of sub-micron vaterite calcium carbonate nanoparticles that are stable in biological media. Two different methods wherein particle nucleation and cluster growth could be effectively controlled was demonstrated to obtain the desired size ranges and crystal phases of calcium carbonate nanoparticles. For the first time, we have demonstrated the capability of modulating the pH *in vivo* of solid tumors using nano-$CaCO_3$. Efficient alkalinization of the acidic pH of tumors depends on particle size. Our results suggest that large (>300 nm) and small (<20 nm) particles are less effective in increasing the *in vivo* pH because of limited diffusion and transient retention in the tumor environment, respectively. The ability of nano-$CaCO_3$ to inhibit tumor growth *in vivo* could serve as a treatment paradigm for long-term tumor static therapy. Future studies will focus on dose optimization, enhancement of tumor-targeting capability, determination of synergistic treatments with complementary therapies, assessment of potential tumor cell reprogramming following nano-$CaCO_3$ treatment, and exploration of the effects of nano-$CaCO_3$ on metastatic growth. Although we did not observe any gross toxicity, multiple injections of the nanoparticles could alter the functional status of some enzymes or pH-sensitive tissues. Future studies will determine these potential effects in a dose escalation study. In addition, we putatively attributed the average pH values measured with the invasive pH electrode to predominantly the pHe of tumors. Validation of this assumption with a noninvasive method that measures the pHe of tumors more accurately[34] will be needed.

Experimental

Simulation of $CaCO_3$ dissolution *in vivo*

Simulations were run in MATLAB using a numerical iteration approximation. Eqn (1–6) are derived from a tissue cylinder model of diffusion and diffusion of $CaCO_3$ from a nanoparticle under the conditions of constant infusion. Eqn (5) and (6) were used to determine the initial $CaCO_3$ and pH distributions in the tissue cylinder model. Changes in $CaCO_3$ and pH were then numerically approximated using eqn (3) and (4). Authors will provide code for the simulation upon on request.

$$CaCO_3(s) \leftrightharpoons Ca^{2+} + CO_3{}^{2-} (k_{a1} = 4.45 \times 10^{-7}) \quad (1a)$$

$$H_2O + HCO_3{}^- \leftrightharpoons H_3O^+ + CO_3{}^{2-} (k_{a2} = 4.69 \times 10^{-11}) \quad (1b)$$

$$H_2O + H_2CO_3 \leftrightharpoons H_3O^+ + HCO_3{}^- \quad (1c)$$

$$C_b = \sqrt{\frac{K_{sp}}{\frac{K_{a1} \times K_{a2}}{\left((10^{-pH})^2 + K_{a1}10^{-pH} + K_{a1}K_{a2}\right)}}} \quad (2)$$

$$\begin{aligned} J &= -D\frac{dC}{dx} \rightarrow \frac{\partial C}{\partial t} = \frac{A}{V}D\frac{(C_s - C_b)}{d} \rightarrow \frac{\partial m}{\partial t} \\ &= AD\frac{(C_s - C_b)}{d} \rightarrow \frac{\partial r_p}{\partial t} = \frac{D}{\rho}\frac{(C_s - C_b)}{d} \end{aligned} \quad (3)$$

$$\frac{dpH}{dt} = -\frac{D}{B}\frac{(C_s - C_b)}{d} \times \frac{1}{L} \quad (4)$$

$$[CaCO_3] = \frac{R_{cmax}}{4D_c}\left(r_c{}^2 - r^2\right) + \frac{R_{cmax}r_c{}^2}{2D_c}\ln\left|\frac{r}{r_c}\right| + k \cdot C_d \quad (5)$$

$$[H^+] = \frac{R_{pmax}}{4D_p}\left(r^2 - r_c{}^2\right) + \frac{R_{pmax}r_c{}^2}{2D_p}\ln\left|\frac{r_c}{r}\right| + 10^{-7.4} \quad (6)$$

The solubility of $CaCO_3$ (C_b), in eqn (2) is a function of pH, the solubility product (K_{sp}), and equilibrium constants K_{a1} and K_{a2}, obtained from eqn (1a and 1b). The rate of change in $CaCO_3$ concentration (C) and in particle radius (r), seen in eqn (3), are derived from Fick's law, and is a function of the diffusion coefficient (D), the surface area of diffusion (A), the distance of diffusion (d) estimated at 0.1 mm, the solubility of $CaCO_3$ (C_b), the volume of the tissue cylinder (C), and the concentration of $CaCO_3$ *in vivo* (C_s). For eqn (4), we simplified eqn (3) by approximating A/V to $1/L$, where L is the length of the tissue cylinder, estimated at 1 mm. The change in concentration of protons can then be converted to a change in a pH of a buffer by dividing by buffering constant, B = 28 mM per pH.[35]

For eqn (5), R_{cmax} was empirically determined by starting at the maximum degradation rate in the tissue at pH of 6.65 and then multiplying by a correction factor until the distribution of $CaCO_3$ appeared optimal, in this case approximately 0.5 mm from the capillary. The resulting degradation correction factor was used throughout for simulating $CaCO_3$ degradation. The radius of the capillary (r_c) was set at 10 μm. The partition coefficient (k) of the capillary is dependent on the capillary pore radius, estimated at 500 nm and particle radius, defined as 100 nm. The initial concentration of $CaCO_3$ (C_d) in the capillary was estimated as 5% of the infused concentration (set as 1 mg in a 20 g mouse).

R_{pmax} was empirically determined as the point at which the average pH in the tissue was 6.65, identified as 0.0225 M s^{-1}. The diffusion coefficient (D_p) was estimated as the diffusion of a particle with a molecular weight of 1 Da in an extracellular matrix. We used the following constants for the simulation based on literature values or model assumptions: r = 50 nm, $K_{a1} = 4.45 \times 10^{-7}$, $K_{a2} = 4.69 \times 10^{-11}$, $K_{sp} = 6 \times 10^{-9}$, M = 100.0869 g mol^{-1}, ρ = 2.71 g mL^{-1}.

Synthesis of 100 nm nano-$CaCO_3$

We synthesized 100 nm $CaCO_3$ nanoparticles using a gas diffusion method. $CaCl_2{\cdot}6H_2O$ (220 mg) was dissolved by

vortexing in anhydrous ethanol (50 mL). The resulting solution was transferred to a 100 mL beaker covered with parafilm. After puncturing small holes in the parafilm, the beaker was placed in a desiccator (with drierite) surrounded by four 20 mL vials containing excess dry ammonium bicarbonate (~9–10 g). The entire system was placed under vacuum for 25 h. The particles were centrifuged at 6800*g* for 10 min, excess ethanol decanted, and the residue was left to dry in the open air before use.

Synthesis of 20 and 300 nm $CaCO_3$

A double decomposition reaction was used to prepare the $CaCO_3$ particles by mixing 0.1 M each of $CaCl_2{\cdot}2H_2O$ and $NaHCO_3$ at room temperature. The premix solutions of $CaCl_2{\cdot}2H_2O$ and $NaHCO_3$ were prepared in water and polyethylene glycol (1 : 5 v/v; average molecular weight 1450 Da) for ~20 nm, and water and ethylene glycol (1 : 5 v/v; molecular weight 62.07 g mol^{-1}) for ~300 nm particles. The synthesized $CaCO_3$ particles were collected by sequentially washing the product with ethanol, methanol and acetone, followed by drying at 60 °C for 1 h.

Transmission electron microscope (TEM)

TEM micrographs were obtained using an FEI Spirit TEM (Hillsboro, USA) operated at 120 kV. A 400-mesh Formvar® carbon-coated copper grid was glow-discharged in a vacuum evaporator (Denton, Moorestown, New Jersey) for 30 s. The sample was prepared by placing 2 μL of sonicated $CaCO_3$ nanoparticles solution onto the grid and wicking off the excess sample with filter paper after 30 s. Alternatively, for EtOH or DMSO solvent-based solutions, 3 μL of particle solution were placed on the grid and left to dry out at room temperature or with the aid of a heat gun.

X-Ray diffraction (XRD)

XRD patterns were obtained by using the Bruker d8 Advance X-ray diffractometer (Bruker, USA) configured with a Cu X-ray tube with 1.5418 Å for analysis of powder samples using LYNXEYE_XE detector. For the analysis, fine acetone ground $CaCO_3$ nanoparticles were kept on a Zero Diffraction Plate (MTI Corporation, USA). XRD data were scanned from 20–60 degrees, with a 0.04 degree step size, a 0.5 s per step count time, with sample rotation turned on (15 rotations per min), with a coupled two-theta/theta scan. The Bruker Diffrac. Eva program was used for the evaluation and processing of X-ray diffraction scan data. Search-match operations included search by DI list, by name, using chemistry filters, and creating an International Centre for Diffraction Data (ICCDD PDF) database filter.

Hydrodynamic diameter and electro-kinetic zeta potential

The to study agglomeration kinetics of $CaCO_3$ nanoparticles, hydrodynamic diameter (D_h) was measured using DLS (Malvern Instruments, Southborough, Massachusetts). Agglomeration kinetics were measured on the basis of data obtained from TR-DLS.

The zeta potential was measured using a Malvern Zetasizer Nano ZS instrument. An applied voltage of 100 V was used for the nanoparticles. A minimum of three measurements were made per sample.

Identification of stable aqueous medium for nano-$CaCO_3$

Nano-$CaCO_3$ was resuspended in the following solvents: (1) dIH_2O; (2) Dulbecco's PBS, (3) PBS, 1 mM $CaCl_2$, and 1 mM $MgCl_2$; (4) PBS, $CaCl_2$, $MgCl_2$ and 2% bovine serum albumin; (5) fetal bovine serum (FBS); and (6) a solution consisting of 20% (PBS, $CaCl_2$, $MgCl_2$, and 2% bovine serum albumin) in 80% FBS. The results of particle stability were analyzed by TR-DLS for up to 7 h, TEM under aqueous conditions, TEM under serum, and XRD after 7 h.

Determination of pH change in acidic media *versus* normal media

We determined $CaCO_3$ dissolution over time by measuring pH changes in conditioned acidic media and fetal bovine serum. Conditioned media was from a 7 day incubation of media with HT1080 cells and an initial pH ~ 6.2. Final concentrations of $CaCO_3$ in the cell free solutions were controlled at 0.67 mg mL^{-1}. $CaCO_3$ was added to conditioned media or serum in ~10 μL of aqueous vector (PBS + $CaCl_2$ + $MgCl_2$ + 2% bovine serum albumin) under hypoxic 5% CO_2 conditions. The pH was then measured after 1 h.

Determination of nano-$CaCO_3$ dose-dependent pH changes in HT1080 cell culture medium

HT1080 cells were plated at 10^5 cells per well in a 24 well plate overnight under hypoxic conditions (0.3% O_2 and 5% CO_2), and then incubated with increasing amounts of 20 nm, 100 nm and 300 nm particles for 24 and 96 h. The particles were directly added and resuspended in media *via* vortexing under hypoxic conditions (0.3% O_2 and 5% CO_2). The pH was measured after 24 and 96 h incubation. n = 3 for each sample.

Animal studies

All animal studies were conducted in accordance with protocols approved by the Washington University Animal Studies Committee. Mice were purchased from Charles River Laboratory.

Determination of pH changes *in vivo* post bolus particle intravenous injection. HT1080 tumors were grown subcutaneously in dorsal flanks of athymic nude mice, in dorsal bilateral flanks. Tumors generally grew in one flank. When the tumors growth reaches approximately 50 mm^3 or greater, the pH was measured using an external pH electrode. Prior to these experiments, the mice had daily I.V. $CaCO_3$ (1 mg) treatments for 3 weeks. Treatments were discontinued for at least 5 days before performing the *in vivo* pH measurements. The average initial pH was 6.94 ± 0.147.

The pH electrode was calibrated before implanting into the tumor and measurements were recorded following a 15-minute equilibration period after implantation. About 1 mg of

each size of particles (20 nm, 100 nm, 300 nm) in a 100 μL solution consisting of PBS, $CaCl_2$, $MgCl_2$ and 2% bovine serum albumin was injected intravenously in individual mice. Approximately 100 μL of aqueous vector (PBS, $CaCl_2$, $MgCl_2$, and 2% bovine serum albumin), 100 μL of 0.84% sodium bicarbonate in deionized (dI) water, and 100 μL of 7.5% sodium bicarbonate in dI water were each serially injected intravenously into the same mouse with 1 h gaps for measurement. Tumor sizes at time of injection for this experiment were 12 mm × 9 mm (20 nm particles), 13.7 mm × 12.5 mm (100 nm), 13.5 mm × 15.5 mm (300 nm), 12.5 × 16.5 mm (.84% bicarbonate), 12.5 × 16.5 mm (7.5% bicarbonate), and 12.5 × 16.5 mm (vector). In general, the pH was then followed each minute for a minimum of 1 h, or up to 3 h if any changes were seen. Animals could tolerate this pH measurement procedure for approximately 4 h and exhibits complete recovery after treatment. Bleeding, if any, was also noted.

Measurement of pH increases post multiple injections. HT1080 tumors were grown subcutaneously in the dorsal bilateral flanks of athymic nude mice. Typically, tumors grew in one flank. When grown to approximately 8.5 mm × 8.5 mm, pH was measured using an external pH electrode. The pH was measured initially following a 15 min equilibration period post probe entry. About 100 μL of 1 mg particles (100 nm) in a solution of PBS, $CaCl_2$, $MgCl_2$, and 2% albumin was injected I.V. every hour for 3 h. The pH was measured continuously throughout.

Determination of tumor growth after $CaCO_3$ administration. HT1080 tumors were grown subcutaneously in the dorsal flanks of six athymic nude mice (age ~8–10 weeks). After tumor growth reached about 100 mm^3, I.V. treatment with nano-$CaCO_3$ was initiated for three mice. About 1 mg of particles (100 nm) in 100 μL of a solution consisting of PBS, $CaCl_2$, $MgCl_2$, and 20 mg mL^{-1} of albumin was injected I.V. every 24 h for 5 days in three mice. The tumor size was measured for each day concurrently between treated and control for 12 days. The pH in the tumor region was then measured for each mouse as described above. During analysis, tumors that were considered too small to measure but deemed palpable, were assigned the largest size measured on Day 1 (50 mm^3) as a conservative estimate.

Acknowledgements

We thank G. Sudlow for assistance in animal care, I.V. animal injections, and tumor model development; Jason Mills for discussions on tumor cell biology; R. Tang, M. Zhou, N. Kotagiri, and K. Black for help with discussion on synthesis and experimental design; and Jin-Yu Shao, for his help with the simulation development. Authors appreciate the help and resources provided by the NSF Funded Nano Research Facility, Washington University in St. Louis for electron microscopy, DLS and XRD facilities. AS was supported by the NCI Ruth Kirschstein Fellowship F30 CA189435 and the Medical Scientist Training Program at Washington University. This work was supported in part by grants from the US National Institutes of Health (R01 CA171651, R01 EB007276, R01 EB021048, U54 CA199092 and P50 CA094056).

Notes and references

1 M. Bellone, A. Calcinotto, P. Filipazzi, A. De Milito, S. Fais and L. Rivoltini, The acidity of the tumor microenvironment is a mechanism of immune escape that can be overcome by proton pump inhibitors, *Oncoimmunology*, 2013, **2**, e22058.

2 I. F. Robey, B. K. Baggett, N. D. Kirkpatrick, D. J. Roe, J. Dosescu, B. F. Sloane, A. I. Hashim, D. L. Morse, N. Raghunand, R. A. Gatenby and R. J. Gillies, Bicarbonate increases tumor pH and inhibits spontaneous metastases, *Cancer Res.*, 2009, **69**, 2260–2268.

3 P. M. J. M. Marion Stubbs, J. R. Griffiths and C. Lidsay, Bashford Causes and Consequences of tumour acidity and implications for treatment, *Mol. Med. Today*, 2000, **6**, 15–19.

4 I. F. Robey and L. A. Nesbit, Investigating mechanisms of alkalinization for reducing primary breast tumor invasion, *Biomed. Res. Int.*, 2013, **2013**, 485196.

5 A. Calcinotto, P. Filipazzi, M. Grioni, M. Iero, A. De Milito, A. Ricupito, A. Cova, R. Canese, E. Jachetti, M. Rossetti, V. Huber, G. Parmiani, L. Generoso, M. Santinami, M. Borghi, S. Fais, M. Bellone and L. Rivoltini, Modulation of microenvironment acidity reverses energy in human and murine tumor-infiltrating T lymphocytes, *Cancer Res.*, 2012, **72**, 2746–2756.

6 D. Neri and C. T. Supuran, Interfering with pH regulation in tumours as a therapeutic strategy, *Nat. Rev. Drug Discovery*, 2011, **10**, 767–777.

7 C. T. Supuran, Inhibition of carbonic anhydrase IX as a novel anticancer mechanism, *World J. Clin. Oncol.*, 2012, **3**, 98–103.

8 M. R. Amin, G. N. Postma, P. Johnson, N. Digges and J. A. Koufman, Proton pump inhibitor resistance in the treatment of laryngopharyngeal reflux, *Otolaryngol. – Head Neck Surg.*, 2001, **125**, 374–378.

9 J. S. Logue and D. K. Morrison, Complexity in the signaling network: insights from the use of targeted inhibitors in cancer therapy, *Genes Dev.*, 2012, **26**, 641–650.

10 N. K. Martin, I. F. Robey, E. A. Gaffney, R. J. Gillies, R. A. Gatenby and P. K. Maini, Predicting the safety and efficacy of buffer therapy to raise tumour pHe: an integrative modelling study, *Br. J. Cancer*, 2012, **106**, 1280–1287.

11 A. Schroeder, D. A. Heller, M. M. Winslow, J. E. Dahlman, G. W. Pratt, R. Langer, T. Jacks and D. G. Anderson, Treating metastatic cancer with nanotechnology, *Nat. Rev. Cancer*, 2012, **12**, 39–50.

12 S. Yang and S. May, Release of cationic polymer-DNA complexes from the endosome: A theoretical investigation of the proton sponge hypothesis, *J. Chem. Phys.*, 2008, **129**, 185105.

13 Y. Ueno, H. Futagawa, Y. Takagi, A. Ueno and Y. Mizushima, Drug-incorporating calcium carbonate nanoparticles for a new delivery system, *J. Controlled Release*, 2005, **103**, 93–98.
14 W. Jinhuan, C. Tuckyun, T. Bing, X. Haoming, X. Zhouhao, C. Zhenhua, F. Yong, C. Wei, X. Anwu, W. Shenming and J. Luo, The inhibition of human bladder cancer growth by calcium carbonate/CalP6 nanocomposite particles delivering AIB1 siRNA, *Biomaterials*, 2013, **34**, 1246–1354.
15 S. Bialkowski, *Use of Acid Distributions in Solubility Problems*, 2004; Available from: http://ion.chem.usu.edu/~sbialkow/Classes/3600/alpha/alpha3.html.
16 R. E. Beck and J. S. Schultz, Hindered Diffusion in Microporous Membranes with known pore geometry, *Science*, 1970, **170**, 1302–1305.
17 K. Greish, Enhanced Permeability and Retention (EPR) Effect for Anticancer Nanomedicine Drug Targeting, in *Cancer Nanotechnology Methods and Protocols*, 2010, pp. 25–37.
18 Y. Svenskaya, B. Parakhonskiy, A. Haase, V. Atkin, E. Lukyanets, D. Gorin and R. Antolini, Anticancer drug delivery system based on calcium carbonate particles loaded with a photosensitizer, *Biophys. Chem.*, 2013, 11–15.
19 S. K. Kim, M. B. Foote and L. Huang, Targeted delivery of EV peptide to tumor cell cytoplasm using lipid coated calcium carbonate nanoparticles, *Cancer Lett.*, 2013, **334**, 311–318.
20 A. Cai, X. Xu, H. Pan, J. Tao, R. Liu, R. Tang and K. Cho, Direct Synthesis of Hollow Vaterite Nanospheres from Amorphous Calcium Carbonate Nanoparticles via Phase Transformation, *J. Phys. Chem. C*, 2008, **112**, 11324–11330.
21 K. L. Haibao Peng, W. Ting, W. Jin, W. Jiao, Z. Rongrong, S. Dongmei and W. Shilong, Preparation of hierarchical mesoporous $CaCO_3$ by a facile binary solvent approach as anticancer drug carrier for etoposide, *Nano Express*, 2013, 321.
22 G. B. Sukhorukov, D. V. Volodkin, A. M. Günther, A. I. Petrov, D. B. Shenoy and H. Mühwald, Porous calcium carbonate microparticles as templates for encapsulation of bioactive compounds, *J. Mater. Chem.*, 2004, **14**, 2073.
23 D. G. Zhongping Zhang, Z. Hui, X. Chenggen, G. Guijian and S.-H. Y. Dapeng Wang, Biomimetic Assembly of Polypeptide-Stabilized CaCO3 Nanoparticles, *J. Phys. Chem.*, 2006, **110**, 8613–8618.
24 S. F. Chen, H. Colfen, M. Antonietti and S. H. Yu, Ethanol assisted synthesis of pure and stable amorphous calcium carbonate nanoparticles, *Chem. Commun.*, 2013, **49**, 9564–9566.
25 D. Kralj and L. Brecevic, Vaterite growth and dissolution in aqueous solution: Kinetics of crystal growth, *J. Cryst. Growth*, 1990, **104**, 793–800.
26 S.-H. Y. Shao-Feng Chen, J. Jiang, F. Li and Y. Liu, Polymorph Discrimination of $CaCO_3$ Mineral in an Ethanol/Water Solution: Formation of Complex Vaterite Superstructures and Aragonite Rods, *Chem. Mater.*, 2006, **18**, 115–122.
27 P. J. Smeets, K. R. Cho, R. G. Kempen, N. A. Sommerdijk and J. J. De Yoreo, Calcium carbonate nucleation driven by ion binding in a biomimetic matrix revealed by in situ electron microscopy, *Nat. Mater.*, 2015, **14**, 394–399.
28 M. H. Nielsen, S. Aloni and J. J. De Yoreo, In situ TEM imaging of CaCO3 nucleation reveals coexistence of direct and indirect pathways, *Science*, 2014, **345**, 1158–1162.
29 D. Gebauer, A. Völkel and H. Cölfen, Stable prenucleation calcium carbonate clusters, *Science*, 2008, **322**, 1819–1822.
30 R. Demichelis, P. Raiteri, J. D. Gale, D. Quigley and D. Gebauer, Stable prenucleation mineral clusters are liquid-like ionic polymers, *Nat. Commun.*, 2011, **2**, 590.
31 B. Jennings and K. Parslow, Particle size measurement: the equivalent spherical diameter, *Proc. R. Soc. London, Ser. A*, 1988, **419**, 137–149.
32 I. M. K. Sam Katz, Interactions of Calcium with Serum Albumin, *Arch. Biochem. Biophys.*, 1953, **44**, 351–361.
33 F. A. Gallagher, M. I. Kettunen, S. E. Day, D. E. Hu, J. H. Ardenkjaer-Larsen, R. Zandt, P. R. Jensen, M. Karlsson, K. Golman, M. H. Lerche and K. M. Brindle, Magnetic resonance imaging of pH in vivo using hyperpolarized 13C-labelled bicarbonate, *Nature*, 2008, **453**, 940–943.
34 N. W. Lutz, Y. L. Fur, J. Chiche, J. Pouyssegur and P. J. Cozzone, Quantitative in vivo characterization of intracellular and extracellular pH profiles in heterogeneous tumors: a novel method enabling multiparametric pH analysis, *Cancer Res.*, 2013, **73**, 4616–4627.
35 P. A. Schornack and R. J. Gillies, Contributions of cell metabolism and H+ diffusion to the acidic pH of tumors, *Neoplasia*, 2003, **5**, 135–145.